Article Type: Research article

Title: Engineered probiotics that sequester arsensite in a mouse gastrointestinal system

Authors and Affiliations:

Nhu Nguyen [1,‡], Miaomiao Wang [1,‡], Sithembiso S. Msibi [2], Vincenzo Kennedy [1], Fateme Esmailie [1], L. Joseph Su [2], Lin Li [1], Clement T. Y. Chan [1,3,*]

[1] Department of Biomedical Engineering, University of North Texas, Denton, TX, USA

[2] Peter O'Donnell Jr. School of Public Health, UT Southwestern Medical Center, Dallas, TX, USA

[3] BioDiscovery Institute, University of North Texas, Denton, TX, USA

[‡] These authors are considered to have equal contributions to this study

* Corresponding author

Supplementary Materials:

One supplementary file is included in this submission:

Supplementary Materials—Containing **Supplementary Figures S1 to S7**

Abstract:

Chronic exposure to inorganic arsenic remains a major global health concern, as arsenite is frequently present in contaminated food and drinking water and readily absorbed through the gastrointestinal (GI) tract. Once internalized, arsenite accumulates in tissues and contributes to long-term health effects, including cancer, organ dysfunction, and neurological disorders. Despite extensive efforts to reduce environmental contamination, there are currently no practical strategies to prevent dietary arsenite from entering the human body during digestion. Here, we report a synthetic biology–based approach that uses engineered probiotics to detect and sequester arsenite directly within the GI tract before systemic absorption occurs. We engineered *Escherichia coli Nissle 1917* (*EcN*), a probiotic strain, to function as a living arsenite-interception system. Central to this design is an arsenite-responsive genetic toggle switch that activates chelator expression upon exposure and sustains production under biostatic conditions, while automatically shutting off during active cell division to limit metabolic burden and enhance biosafety. In parallel, we engineered an arsenite-binding protein derived from the transcriptional regulator ArsR to eliminate DNA-binding activity while retaining high-affinity metal binding,

yielding a non-toxic chelator suitable for intracellular sequestration. The resulting engineered strain efficiently removed arsenite from its surrounding environment in vitro while maintaining robust cell viability and growth. To translate these findings to an in vivo context, we developed a mass-transfer model describing arsenite distribution among the stomach lumen, engineered bacteria, and epithelial cells. This model guided the selection of a bacterial dose predicted to substantially deplete lumenal arsenite prior to epithelial uptake. Using this strategy, we demonstrated in a mouse GI model that oral administration of engineered *EcN* markedly reduced arsenite entry into the bloodstream compared with wild-type EcN or no-bacteria controls. Together, these results establish a programmable probiotic platform for intercepting dietary arsenite and highlight a potential strategy for preventing absorption of environmental toxicants using living microbial therapeutics.

Introduction:

Heavy metal contamination represents a critical global health challenge. Inorganic arsenic, such as arsenite, is one of the most prevalent toxic metal species, with chronic exposure linked to cancers, organ failure, neurodegeneration, and other severe diseases (*1, 2*). As arsenite is hard to be eliminated once absorbed into human tissues, their effects are cumulative and long-lasting, and no safe threshold of exposure exists. Nonetheless, heavy metals remain abundant in human diets worldwide; more than 140 million people are estimated to consume arsenite-contaminated drinking water (*3*), millions in the United States are at risk from unsafe arsenite concentrations (*4*), and staple crops such as rice and wheat frequently contain high levels of arsenite (*5-7*). Despite the magnitude of this problem, there remains limited strategies to protect individuals from dietary exposures to this heavy metal species effectively. Thus, new approaches are urgently needed to mitigate this increasing health burden.

Current strategies to limit exposure focus on environmental management and monitoring. Approaches such as phytoremediation of contaminated soils (*8*) , improved irrigation and waste practices (*9, 10*), and inspection programs supported by analytical techniques like mass spectrometry (*11, 12*) and atomic absorption spectroscopy (*13-15*) have value but are costly, infrastructure-dependent, and insufficient in regions with widespread contamination. Water purification systems can reduce exposure but remain inaccessible for many populations, and importantly, no practical technologies exist to prevent heavy metal uptake from food. Chelation therapy, while effective in acute poisoning, cannot be used preventively because of many adverse side effects caused by chelating agents (*16*). These limitations highlight an urgent need for affordable and scalable solutions to block dietary heavy metal absorption.

Microbial systems offer a promising foundation to tackle this health problem. Engineered bacteria expressing protein-based chelators such as metallothioneins (*17-19*), phytochelatins (*20*), and ArsR (*21*) can sequester toxic metals, and peptides with high binding affinity have been designed for similar purposes (*22-24*). In parallel, transcriptional regulators that sense specific metals have been harnessed for biosensing applications (*25-28*); recent innovations in directed evolution (*29, 30*) and genetic circuit amplification (*31*) have shown promising paths to expand sensitivity. However, most efforts have centered on detection rather than incorporating genetic sensing with biological chelators to promote heavy metal removal.

Emerging synthetic biology approaches have been explored to engineer gut microbes as versatile living therapeutics. Probiotic strains have been developed to metabolize harmful molecules, suppress pathogens, and secrete bioactive molecules to improve host physiology (*32-37*). These advances demonstrate that gut microbes can be designed to sense environmental or host-derived signals and deliver therapeutic responses in situ.

Here, we have explored the concept of microbial sense-and-response for an environmental toxicology application by engineering gut bacteria to detect and sequester arsenite in the gastrointestinal tract before absorption occurs. A key advantage of engineered bacteria is their ability to couple sensing and intervention in real time. Unlike conventional chelator therapies, which bind both toxic and essential metals, engineered microbes can be designed to activate metal-binding only when a target contaminant is present, thereby reducing off-target effects and minimizing disruption of essential metal homeostasis. This dynamic, conditional response also allows bacteria to conserve resources for their cell fitness in the drastically changing gastrointestinal environment yet rapidly increase sequestration capacity during exposure events. Together, these features provide a unique platform for selective, preventative detoxification that is not achievable with existing chemical or physical methods.

Specifically, we have developed an *Escherichia coli Nissle 1917* (*EcN*) strain equipped with an arsenite-responsive genetic circuit to control an output module to express a protein-based arsenite chelator. We demonstrated that this engineered bacterial strain performed in a mouse gastrointestinal system to reduce the rise in blood arsenite levels after an oral administration of arsenite solution. This work establishes a new preventative strategy against dietary metal exposure and broadens potential applications of engineered microbes to include protection from environmental toxicants.

Results:

Design of genetic circuit for sensing and responding to arsenite

For protection against dietary arsenite, we designed an engineered strain of *EcN* that can pass through the digestive tract, capture the toxic metal, and be excreted while retaining the bound arsenite. The strain was designed to express a protein-based arsenite chelator, enabling bioaccumulation of arsenite-protein complexes within bacterial cells. A key feature of our design is that the bacteria will produce a basal level of chelator even in the absence of heavy metals, ensuring they are primed to capture toxicants as soon as exposure occurs. This basal level is intentionally kept low to minimize non-specific binding of essential metal ions and to preserve cellular fitness. Upon encountering arsenite, the genetic circuit triggers a robust induction of chelator expression, dynamically reallocating cellular resources to maximize sequestration at the point of highest toxicant burden. Notably, the circuit is further designed to sustain elevated chelator expression in arsenite-exposed cells even after arsenite levels decline, ensuring effective clearance of residual toxicants and extending the protective effect during digestion.

The engineered *EcN* cells are intended for repeated oral administration and most cells will be eliminated from the gastrointestinal tract after passage; however, a small fraction may persist and colonize the gut for extended periods (*38*). To prevent these proliferating cells from uncontrollably producing the chelator in the absence of arsenite, we incorporated a growth-dependent control feature. When arsenite concentrations fall below the detection threshold, chelator synthesis continues only in non-dividing cells; active cell division over several cycles leads to the cessation of chelator expression.

This event-triggered, sustained response is enabled by a genetic toggle switch architecture (**Figure 1**). Although the ArsR transcriptional regulator functions as an arsenite sensor (*39*), directly coupling output expression to ArsR activity restricts both sensitivity and the duration of response. To overcome these limitations, we implemented reciprocal repression between ArsR and a counter-regulator, CelR—a transcriptional repressor that controls gene expression from an engineered promoter (*40*). In the absence of arsenite, ArsR dominates the regulatory circuit and represses both the chelator and CelR. Upon

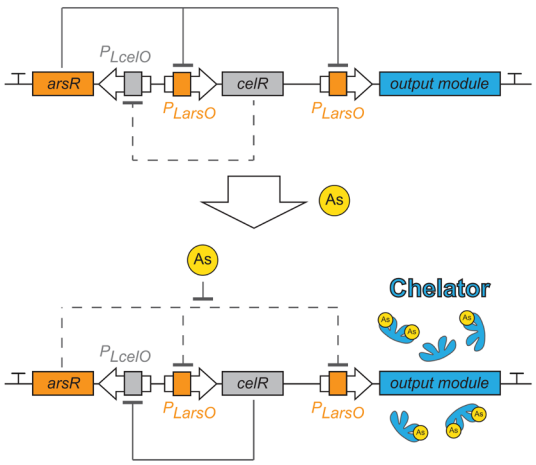

Figure 1. Circuit design for sensing and responding to arsenite. The circuit consists of two regulatory proteins, ArsR and CelR, that form a toggle switch. Under normal growth conditions without arsenite, ArsR is highly expressed and dominant, maintaining the circuit in the chelator-OFF state. Upon arsenite exposure, CelR and chelator expressions are induced, which represses *arsR* transcription. Once triggered, chelator expression continues even after arsenite is removed, until active cell division reduces CelR levels and restores ArsR expression, returning the circuit to the OFF state.

137 arsenite exposure, ArsR repression is relieved, allowing expression of both genes; newly
138 synthesized CelR then suppresses ArsR, reinforcing the ON state. This architecture confers two
139 key advantages. First, it enables a prolonged response: because CelR continues to inhibit ArsR
140 after arsenite levels fall, chelator expression persists, supporting clearance of residual toxicants.
141 Second, it enhances sensitivity: by lowering ArsR abundance through CelR-mediated
142 repression, the circuit reduces the arsenite threshold required to fully switch into the ON state.
143 Importantly, the circuit also incorporates a mechanism that ties output decay to active cell
144 division. We intentionally limited the maximal intracellular CelR level so that rapid growth dilutes
145 CelR faster than it can repress ArsR, allowing ArsR to regain dominance and gradually return
146 the circuit to the OFF state. Together, these design features transform a transient environmental
147 cue into a durable yet self-limiting detoxification program, establishing a programmable strategy
148 for microbial heavy-metal sequestration in vivo.

149 **Arsenite-responsive toggle switch circuit**

150 To establish the design in **Figure 1** for desired arsenite sensing and response behaviors, we
151 first constructed the Control circuit shown in **Figure 2A** to characterize the transcriptional
152 regulator ArsR as an arsenite-responsive genetic sensor; the circuit was built in a plasmid that
153 can be hosted by *EcN*. The *arsR* gene was placed under the control of the promoter P_{LcelO} (*40*);
154 transcriptional activity of this promoter is repressed by the regulator CelR. In the absence of
155 CelR, ArsR was therefore constitutively expressed in this circuit. ArsR specifically binds to the
156 *arsO* operator (*39*); we incorporated this operator downstream of the P_L promoter (*41*) to
157 generate P_{LarsO} (**Supplementary Figure S1**). Binding of ArsR to this operator represses
158 transcription from the engineered promoter. We next characterized the signal-response behavior
159 of the *arsR*/P_{LarsO} system using mCherry as a fluorescent reporter. *EcN* cells harboring this
160 circuit were exposed to a range of sodium arsenite concentrations (0 to 5 μM) overnight, and
161 mCherry fluorescence was quantified by flow cytometry (**Figure 2B**). In unexposed cells,
162 mCherry fluorescence averaged 975 ± 41 a.u. (mean ± S.D.), whereas exposure to 5 μM
163 arsenite increased fluorescence to 12,237 ± 1,511 a.u., confirming that the system is responsive
164 to arsenite.

165 Next, we constructed the toggle switch by incorporating the *celR* regulator gene into the
166 plasmid, placing it under the control of the P_{LarsO} promoter so that ArsR and CelR mutually
167 repressed each other's expression (Toggle Switch circuit; **Figure 2A**). Our goal was to develop
168 a sense-and-response system in which exposure to arsenite triggers expression of the output
169 gene, and once activated, the output remains expressed even after arsenite is removed, until

170 cells resume active division during
171 growth. Similar growth-dependent
172 toggle switch behavior has been
173 developed previously (*42*).
174 To achieve this functionality in
175 our arsenite-sensing circuit, we fine-
176 tuned CelR expression by
177 modulating its ribosome binding site
178 (RBS) strength across a range of
179 predicted translation efficiencies
180 (*43*). Each circuit variant was
181 evaluated to identify the version that
182 produced the desired response
183 dynamics (**Supplementary Figure**
184 **S1**). For initial screening, cultures
185 were grown overnight in the
186 presence of 0 or 5 μM sodium
187 arsenite to allow full induction of
188 output expression. We sought a
189 circuit variant that exhibited low
190 mCherry expression in the absence
191 of arsenite and strong mCherry
192 induction upon arsenite exposure,
193 consistent with the expected toggle
194 switch behavior. To identify circuit
195 variants capable of sustaining
196 output expression under biostatic
197 conditions after arsenite removal,
198 cells from 5 μM arsenite-exposed
199 cultures were collected and
200 resuspended in an equal volume of
201 fresh culture medium lacking arsenite, thereby maintaining cell density and ensuring a
202 stationary-phase state. These cultures were then incubated under standard growth conditions
203 for 24 hours before mCherry fluorescence was measured.

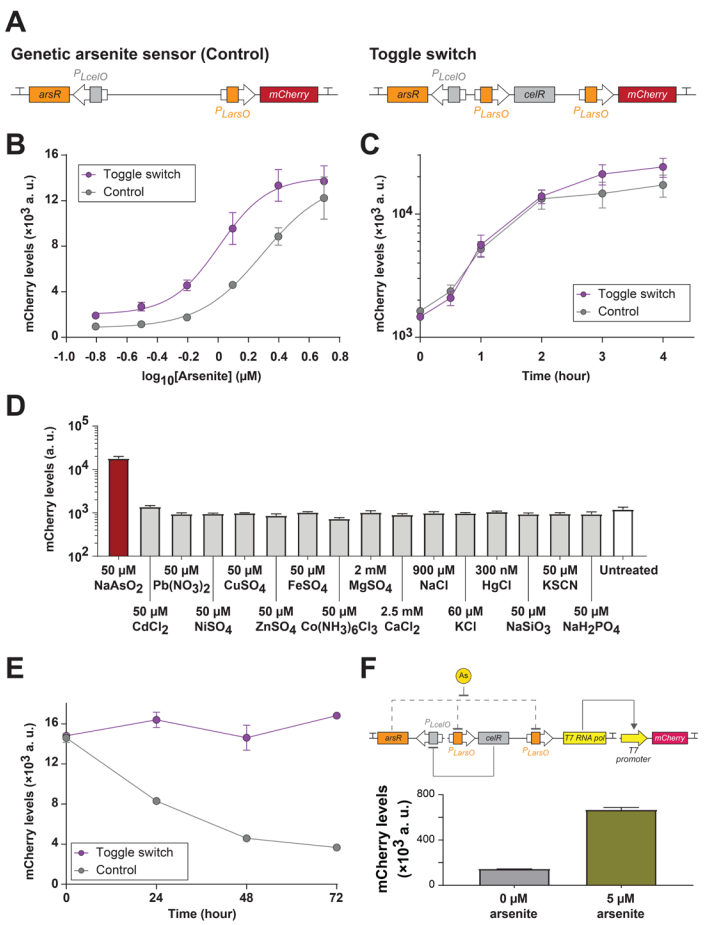

Figure 2. Characterization of the arsenite-responsive toggle switch circuit. (**A**) The circuit design of the Control and Toggle Switch circuits are shown. (**B**) Sensitivity of these two circuits were assessed by measuring cellular response to a 24-hour exposure to 0 to 5 μM arsenite. The equation of illustrated dose-response curves is presented in the Methods section. (**C**) To evaluate the rate of output production, cellular levels of mCherry were measured in 0 to 4 hours of exposing to 5 μM of arsenite. (**D**) Specificity of signal detection was assessed by exposing cells containing the toggle switch circuit to various conditions with different chemical species and measuring changes in cellular mCherry levels. (**E**) Stability of output production was characterized; arsenite-induced cells were transferred to a biostatic condition without arsenite for 72 hours with measurement of cellular mCherry levels every 24 hours. (**F**) To enhance output production levels, the characterized Toggle Switch circuit was used to control the expression of T7 RNA polymerase for driving mCherry production as the output. *EcN* with this circuit was incubated with 0 and 5 μM of sodium arsenite overnight before characterizing cellular mCherry levels. Each data point represents mean ± S.D. of three biological replicates.

204 The mCherry expression levels varied across cells harboring different circuit variants
205 (**Supplementary Figure S1**). When the RBS driving *celR* was too strong (e.g., RBS 1),
206 mCherry fluorescence was high under both 0 and 5 μM arsenite conditions, indicating that
207 excessive CelR expression suppressed *arsR* transcription regardless of arsenite presence.
208 Among the variants exhibiting differential responses between 0 and 5 μM arsenite (RBS 2 to
209 13), most failed to maintain mCherry expression after arsenite removal for 24 hours. In the
210 Control circuit lacking *celR*, mCherry fluorescence decreased from 14,600 ± 367 to 8,297 ± 105
211 a.u. after this biostatic incubation; several toggle switch variants displayed similar behavior,
212 suggesting that these circuits produced insufficient CelR levels to repress ArsR even after
213 arsenite induction. In contrast, the circuit containing RBS 10 maintained high mCherry
214 fluorescence under biostatic conditions following arsenite removal. This variant satisfied our
215 design criteria and was therefore selected for subsequent characterization.

216 **Characterization of circuit response**

217 We compared the arsenite sensitivity of this selected toggle switch circuit with that of the
218 control circuit (**Figure 2B**). Cultures harboring either construct were exposed overnight to a
219 range of sodium arsenite concentrations, and cellular mCherry fluorescence was quantified. The
220 resulting data were fitted to dose-response curves, revealing that the toggle switch enhanced
221 sensitivity to arsenite relative to the control. Specifically, cells carrying the toggle switch reached
222 half-maximal mCherry levels (EC_{50}) at 1.02 μM arsenite, whereas those with the control circuit
223 required 1.97 μM. Furthermore, the Hill slope of the toggle switch response (2.71) was steeper
224 than that of the control circuit (2.09), indicating a more pronounced, cooperative increase in
225 output expression with rising arsenite concentrations. This behavior is consistent with the
226 expected mechanism in which arsenite-induced CelR expression suppresses ArsR, thereby
227 amplifying mCherry expression.

228 Additionally, we monitored how quickly the circuits responded to arsenite exposure (**Figure**
229 **2C**). Both engineered strains were treated with 5 μM sodium arsenite at the mid-log phase, and
230 their mCherry fluorescence was measured over time. A clear increase in fluorescence was
231 detected within the first hour in both cases, indicating that the regulator ArsR rapidly sensed and
232 responded to arsenite. After the initial response, mCherry levels in both strains continued to rise
233 gradually.

234 We next evaluated the specificity of the toggle switch for arsenite detection (**Figure 2D**). In
235 the gastrointestinal environment, the engineered bacteria are likely to encounter a wide variety
236 of ionic species; therefore, it is essential that the circuit responds selectively to arsenite to avoid
237 unnecessary chelator production, which could waste cellular resources and lead to off-target

238 metal sequestration. Engineered *EcN* carrying the toggle switch was exposed to different
239 chemicals containing various cations and anions. Among all tested conditions, cells exposed to
240 50 μM sodium arsenite exhibited a marked increase in mCherry fluorescence (approximately
241 15-fold), whereas cells treated with other ions showed changes of less than 2-fold. These
242 results demonstrate that the toggle switch responds specifically to arsenite and is largely
243 insensitive to other physiologically relevant ions.
244 Furthermore, we examined the stability of output expression after arsenite removal in the
245 engineered *EcN* culture (**Figure 2E**). To prevent uncontrolled chelator production during active
246 growth, our design aimed for a circuit that sustains output expression only under biostatic
247 conditions and halts production when cells resume division. To maintain arsenite-induced cells
248 in a non-growing state, saturated cultures were collected daily and resuspended in an equal
249 volume of fresh medium, replenishing nutrients for cell viability without dilution. This approach
250 preserved high cell density and maintained cells in a biostatic phase. Under these conditions,
251 cells carrying the Control circuit exhibited a sharp decline in mCherry fluorescence after arsenite
252 removal, whereas those harboring the Toggle Switch maintained elevated fluorescence for at
253 least three days. This sustained expression is consistent with CelR-mediated maintenance of
254 the ON state, indicating that the toggle switch confers a form of molecular memory that prolongs
255 output production in the absence of continued arsenite exposure.
256 In contrast, resumption of cell growth triggered the toggle switch to revert to the OFF state
257 (**Supplementary Figure S2**). To examine the effect of cell division on circuit stability, we diluted
258 the cultures 2-, 3-, or 6-fold after each medium exchange, thereby modulating the number of
259 division cycles required for the cultures to reach saturation. In toggle switch cultures subjected
260 to 2-fold daily dilution, mCherry fluorescence decreased only about 2-fold after three days,
261 indicating that output production persisted but at a reduced rate. However, higher daily dilution
262 ratios (3- and 6-fold) led to a more pronounced decline in mCherry levels, consistent with active
263 cell division resetting the circuit to the OFF state. This behavior highlights a key safety feature of
264 the design—ensuring that proliferating cells in the host do not continuously produce excessive
265 levels of the chelator.
266 To further enhance output production, we coupled the Toggle Switch circuit to a T7 RNA
267 polymerase-driven expression module, enabling transcriptional amplification of the output gene
268 (**Figure 2F**). The translation efficiency of T7 RNA polymerase was optimized by tuning its RBS
269 strength (**Supplementary Figure S3**), with sequences designed using the computational RBS
270 calculator (*43*). Each circuit variant was induced with arsenite for 1 hour, and cellular mCherry
271 fluorescence was quantified. Among the tested variants, the construct containing RBS C

272 exhibited the greatest dynamic range, with mCherry fluorescence increasing from 54,481 ±
273 1,409 a.u. (uninduced) to 235,523 ± 7,685 a.u. (induced). When cultures of this variant were
274 incubated overnight to assess maximal output, fluorescence reached 143,220 ± 1,489 a.u. and
275 664,975 ± 18,216 a.u. in uninduced and induced cells, respectively. These results demonstrate
276 that coupling the Toggle Switch to a T7-based transcriptional amplifier markedly boosts output
277 expression. The strong, orthogonal activity of T7 RNA polymerase likely insulates the output
278 expression from host transcriptional system, thereby expanding its dynamic range and
279 enhancing signal fidelity.

280 **Development of an arsenite chelator**

281 ArsR is a transcriptional regulator that responds to arsenite as an inducer and belongs to the
282 ArsR/SmtB family (**Figure 3A**). An ArsR homolog binds arsenite with a dissociation constant of
283 approximately 10^{-15} M, indicating exceptionally tight binding (*44*). Based on this property, we
284 selected ArsR as the chelator for our engineered bacteria. However, high-level expression of
285 ArsR proved toxic to *E. coli* as we demonstrated that overexpression of this gene for three hours
286 under an inducible promoter caused roughly a 2-log reduction in colony-forming units (CFU;
287 **Figure 3B**). Consistent with this observation, previous studies have also reported growth
288 inhibition upon ArsR expression (*45*). We hypothesize that this cytotoxicity arises from non-
289 specific binding of ArsR to genomic DNA; at high intracellular concentrations, ArsR may repress
290 essential genes, thereby compromising cell viability.

291 To test this hypothesis and to develop an arsenite chelator with reduced cytotoxicity, we
292 sought to engineer an ArsR mutant that retains arsenite-binding ability but loses DNA-binding
293 capacity. Members of the ArsR/SmtB family contain a winged helix-turn-helix DNA-binding motif,
294 with helices α3 and α4 directly contacting the major groove of DNA (*46, 47*). The N-terminal
295 region of α3 is also involved in metal chelation (*48, 49*). Our strategy was to disrupt DNA binding
296 while minimizing perturbation of the metal-binding site. To this end, we introduced single amino
297 acid substitutions within residues 42 to 49 of helix α4 of ArsR, a region predicted to mediate
298 DNA interaction but not metal binding based on the protein-DNA complex structure of a family
299 member, NolR (**Figure 3A**), and sequence alignment among ArsR/SmtB family regulators
300 (**Supplementary Figure S4**).

301 Among the ArsR mutants generated, individual amino acid residues were substituted with
302 alanine. Each *arsR* mutant gene was expressed under the control of a T7 promoter in an *E. coli*
303 strain harboring an arabinose-inducible T7 RNA polymerase gene in its genome. To evaluate
304 cytotoxicity, we compared the colony-forming units (CFUs) of cultures with and without induction
305 of *arsR* expression by 0.2% arabinose. Notably, most substitutions alleviated cytotoxicity, except

306 for S47A (**Figure 3B**). Three mutants, including L46A, H48A, and H49A, restored cell growth to

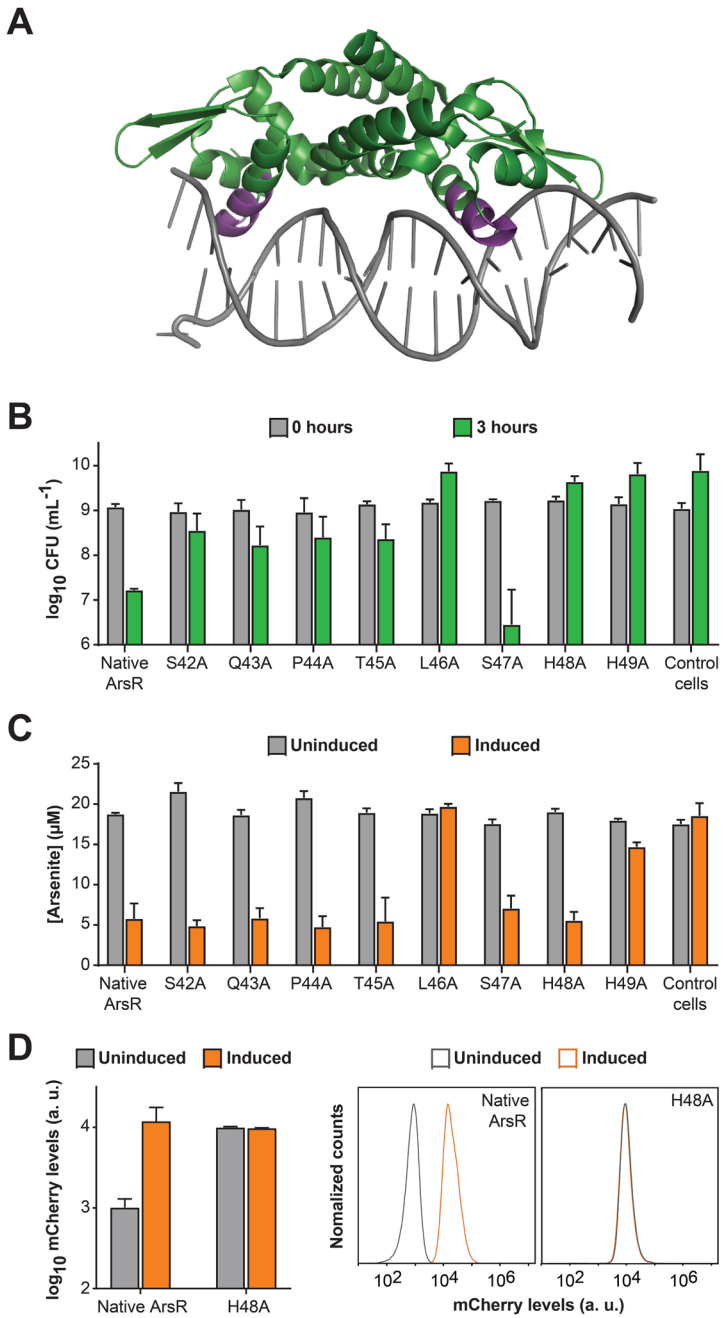

Figure 3. Development of the arsenite chelator. (**A**) Structure of NolR, a ArsR/SmtB family regulator, in complex to a DNA oligonucleotide (PDB:4OMY). The homologous region in α4 (residues 42 to 49) for mutation is colored purple, which situated in the DNA major groove. (**B**) Assessment of cytotoxicity of ArsR mutant expression to *E. coli*. Colony-forming units in each culture was measured before induction (0 hours) and three hours after induction (3 hours). (**C**) Efficiency of arsenite sequestration. Cultures with and without induction for the expression of an *arsR* mutant were incubated with 20 μM sodium arsenite for 3 hours before collection of supernatants for arsenite quantification. (**D**) Characterization of ArsR derivatives in controlling gene expression. ArsR and ArsR H48A were used to control mCherry expression in *E. coli*. After overnight induction with 5 μM arsenite, cells were collected to measure mCherry levels with flow cytometry (left panel). Representative raw data were presented on the right. Each data point represents mean ± S.D. of three biological replicates.

307 levels comparable to the control strain lacking ArsR expression, as determined by CFU
308 measurements.
309 In parallel, we assessed the arsenite sequestration capacity of these strains. Induced and
310 uninduced cultures with each mutant were incubated with 20 μM of sodium arsenite, after which
311 supernatants were collected to quantify residual arsenite levels (**Figure 3C**). Among the three
312 mutants with the lowest toxicity, L46A and H49A mutants exhibited reduced arsenite removal
313 efficiency, whereas the H48A mutant maintained strong arsenite-binding capacity, achieving
314 arsenite reduction comparable to that of native ArsR. Therefore, H48A was selected as the
315 optimized arsenite chelator for subsequent studies.
316 To confirm the loss of DNA-binding function in the H48A mutant, we evaluated its ability to
317 regulate an ArsR-responsive promoter controlling mCherry expression in *E. coli* (**Figure 3D**).
318 The genetic design, shown as the Control circuit in **Figure 2A**, includes a constitutively
319 expressed *arsR* gene that represses mCherry expression as a reporter. In cells expressing
320 native ArsR, mCherry fluorescence increased approximately 10-fold upon arsenite exposure. In
321 contrast, when the native *arsR* gene was replaced by the *arsR H48A* mutant, cells expressing
322 the ArsR H48A mutant exhibited high mCherry expression even in the absence of arsenite, and
323 fluorescence levels remained unchanged after induction. These results indicate that ArsR H48A
324 has lost its DNA-binding capability, consistent with its reduced cytotoxicity.
325 **Engineered *EcN* for arsenite sequestration**
326 After establishing the genetic sense-and-response circuit (**Figure 2**) and the arsenite
327 chelator module (**Figure 3**), we combined these components to construct the final engineered
328 *E. coli Nissle 1917* (*EcN*) strain capable of detecting and sequestering arsenite. In this design
329 (**Figure 1**), the optimized toggle switch controls the expression of the *arsR H48A* chelator gene,
330 enabling the bacteria to activate arsenite capture in response to an arsenite exposure.
331 Before assessing sequestration performance, we examined how this circuit affected cell
332 physiology and growth. Using optical density measurements at 600 nm, we tracked the growth
333 of engineered and wild-type *EcN* strains under both arsenite-free and arsenite-exposed
334 conditions (**Figure 4A**). In the absence of arsenite, cells harboring the toggle switch circuit grew
335 slightly slower than wild-type cells, suggesting that even the basal activity of the circuit imposed
336 a small metabolic cost, which can be due to low-level chelator expression drawing on cellular
337 resources. When exposed to arsenite, the growth rate of toggle switch-containing cells declined
338 further, whereas control cells showed no significant change. This difference indicates that the
339 reduced growth rate was not a direct toxic effect of arsenite, but rather a result of the circuit
340 becoming activated and diverting energy toward chelator production.

To further evaluate the physiological impact of circuit activation, we performed colony-forming unit (CFU) analyses (**Supplementary Figure S5**). After 3.5 hours of arsenite exposure, CFU counts of induced toggle switch cultures were roughly 10-fold lower than those of unexposed controls, consistent with a slowdown in cell growth. However, by 5.5 hours, CFU values reached above 10^9 cells/mL, which is comparable to the other test conditions,

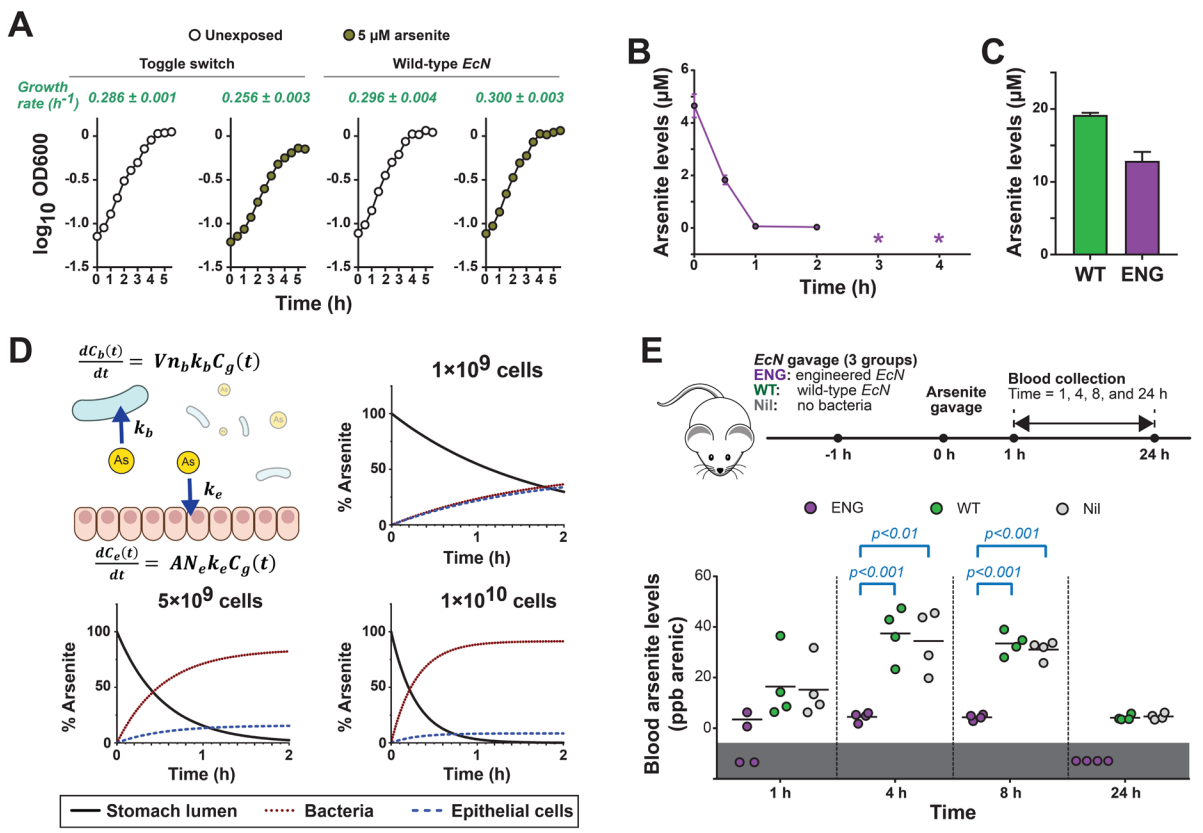

Figure 4. Characterization of engineered EcN for arsenite sequestration. (**A**) Growth of engineered *EcN* harboring the arsenite sense-and-response circuit (ENG) and wild-type *EcN* (WT) was measured by culture absorbance. Calculated growth rates for each strain in the presence of 0 or 5 μM sodium arsenite are shown above the corresponding plots. (**B**) In vitro arsenite sequestration by engineered *EcN* was quantified using ICP-MS. Data points represent the concentration of arsenite remaining in the culture supernatant after arsenite addition at time 0 h. An asterisk (*) indicates that arsenite levels were below the limit of detection at that timepoint. (**C**) Maximum sequestration capacity was assessed by exposing engineered and wild-type *EcN* cultures to 20 μM arsenite and analyzing supernatants after 3 h. For panels A to C, each data point represents the mean ± S.D. of three biological replicates; error bars are omitted when smaller than the marker. (**D**) A mathematical model was constructed to simulate arsenite mass transfer in the stomach lumen. Rate constants for arsenite uptake by engineered bacteria (k_b) and epithelial cells (k_e) were derived from experimental data and literature values. These constants are involved in defining the temporal contributions of bacterial uptake, $C_b(t)$, and epithelial uptake, $C_e(t)$, to changes in luminal arsenite concentration, $C_g(t)$. Vn_b denotes the total number of bacterial cells, and AN_e denotes the total number of epithelial cells. The model, detailed in the Methods, was used to simulate arsenite transfer during the first 2 h following oral gavage of engineered *EcN* and arsenite. (**E**) Blood arsenite levels in mice following bacterial treatment. The timeline (top) indicates the schedule of bacterial administration, arsenite exposure, and blood sampling. In the plot (bottom), each marker represents a data point from an individual mouse; bars denote mean values for four biological replicates. Markers within the gray shaded region indicate samples with undetectable arsenite. Two-way ANOVA revealed significant effects of engineered *EcN* treatment ($F = 22$; $p < 0.001$) and time ($F = 56$; $p < 0.001$). Significant pairwise differences identified by Tukey's HSD are indicated in blue.

346 demonstrating that the engineered *EcN* cells remained viable and capable of sustaining growth
347 even after circuit activation, a critical property for its potential function within the gastrointestinal
348 tract.

349 **In vitro characterization of arsenite sequestration**

350 To reach our goal of using this engineered *EcN* to prevent arsenite absorption in a
351 gastrointestinal tract, we first characterized its arsenite sequestration function in vitro, such that
352 we can use these results to simulate the amount of bacterial cells required in the animal
353 experiments for efficient sequestration. To determine the kinetics of arsenite sequestration in
354 cultures (**Figure 4B**), we exposed cultures at the log phase (OD600 was 0.6 to 0.7) to 5 μM of
355 sodium arsenite and collected samples to measure arsenite concentration in supernatant at
356 different time points. After 0.5 hour of incubation, arsenite levels were reduced to 1.83 ± 0.17
357 μM; based on CFU analysis at the 0- and 1-hour time point, we estimated that there were about
358 4.6×10^{9} cells/mL in the culture for arsenite sequestration (**Supplementary Figure S6**). The
359 initial sequestration rate was calculated as $(1.22 \pm 0.13) \times 10^{-18}$ mol/cell/hour. The levels of
360 arsenite decreased to below 0.1 μM after 1 hour and it was under our detection limit at the 3-
361 hour time point.

362 Beyond sequestration kinetics, we also assessed the arsenite-binding capacity of the
363 engineered *EcN* strain by challenging it with a higher arsenite concentration that exceeded its
364 sequestration potential. Log-phase cultures were exposed to 20 μM sodium arsenite, and
365 residual arsenite levels in the supernatant were measured at 0 and 3 hours. After 3 hours,
366 arsenite concentrations decreased to 12.8 ± 1.0 μM (**Figure 4C**), corresponding to substantial
367 uptake by the bacterial population. At this timepoint, cell density was estimated at (1.05 ± 0.41)
368 $\times 10^{10}$ CFU/mL (**Supplementary Figure S6**), yielding an average arsenite sequestration
369 capacity of $(6.02 \pm 0.97) \times 10^{-19}$ mol/cell. These results quantify the per-cell arsenite retention
370 ability of the engineered *EcN*, providing a useful benchmark for predicting the total detoxification
371 potential achievable in vivo.

372 **Determination of the arsenite dose for mouse studies**

373 After characterizing arsenite sequestration by the engineered bacteria in vitro, we next
374 evaluated their ability to reduce arsenite absorption in a mouse gastrointestinal model. As a first
375 step, we sought to identify an arsenite dose that would generate a detectable but unsaturated
376 increase in blood arsenite levels. An ideal dose should be high enough to produce a measurable
377 rise in blood concentration, yet low enough that a reduction in arsenite availability within the gut
378 (such as through bacterial sequestration) would cause a proportional and significant decrease in

379 blood arsenite levels. In contrast, at saturating doses, arsenite absorption becomes rate-limited,
380 and changes in gut arsenite content would no longer be reflected in the bloodstream.
381 To determine such a dose, mice were orally gavaged with either 1 nmoles or 4 nmoles of
382 sodium arsenite (**Supplementary Figure S7**). At the higher dose (4 nmoles), blood arsenite
383 levels rose rapidly to 181 ± 66 ppb after 1 hour and continued increasing to 306 ± 25 ppb at 8
384 hours, remaining elevated (198 ± 44 ppb) even after 24 hours, indicating systemic saturation
385 and incomplete clearance. In contrast, mice receiving 1 nmole of arsenite exhibited a more
386 dynamic and responsive profile: blood arsenite reached 15 ± 11 ppb at 1 hour, peaked at 34 ±
387 12 ppb by 4 hours (remaining 31 ± 4 ppb at 8 hours), and returned near baseline (4.6 ± 1.2 ppb)
388 at 24 hours.
389 Together, these results indicate that 1 nmol of arsenite provides an optimal dose for
390 evaluating in vivo sequestration, as fluctuations in gut arsenite availability are expected to
391 sensitively mirrored by changes in blood arsenite concentration.
392 **Computational simulations of arsenite transfer in the gastrointestinal model**
393 Based on the in vitro sequestration parameters and the arsenite dose established for mouse
394 studies, we developed a mathematical model to simulate arsenite mass transfer in the
395 gastrointestinal tract. Our goal was to estimate the number of engineered *EcN* cells required to
396 effectively prevent arsenite absorption (**Figure 4D**). The model tracks the time-dependent
397 concentrations of arsenite in the stomach lumen, $C_g(t)$; and the contributions of the loss of
398 arsenite in the stomach lumen by engineered bacterial cells, $C_b(t)$ and the epithelial cells lining
399 the stomach, $C_e(t)$. The system is represented as a short, closed-segment interval with no
400 external inflow or outflow and assumes no efflux, redistribution, or metabolism of arsenite by
401 either bacterial or epithelial cells during the analysis window.
402 A mass balance is applied to the lumen and coupled to first-order uptake terms describing
403 sequestration by bacteria (a volumetric uptake sink) and uptake by epithelial cells (a wall-
404 associated sink). This formulation captures lumenal depletion of arsenite alongside its
405 corresponding accumulation in the two biological sinks. The resulting system of equations,
406 described in the Methods section, provides explicit solutions for arsenite concentrations in each
407 compartment as functions of bacterial load and time. The bacterial uptake rate constant was
408 derived from our experimental measurements (**Figure 4B**), while parameters describing the
409 epithelial compartment, including stomach volume, surface area, and epithelial cell number,
410 were obtained from the literature (*50-53*).
411 Using these inputs, the model simulated how arsenite distributes between epithelial and
412 bacterial cells following oral gavage of 1 nmol arsenite in the presence of varying bacterial loads

413 (1, 5, or 10 $\times 10^9$ cells). The simulations predicted that 1 $\times 10^9$ cells would sequester only ~36%
414 of arsenite within 2 hours, whereas 5 $\times$ 10^9 cells would capture ~82% (**Figure 4D**). Increasing
415 the bacterial dose further to 1 $\times 10^{10}$ cells produced only modest additional benefit (~91%).
416 Based on these simulations, we selected 5 $\times 10^9$ engineered cells as the dose for subsequent
417 mouse experiments, balancing sequestration efficiency with the need to avoid unnecessary
418 physiological stress from excessive bacterial loads.

419 **Effect of engineered *EcN* on blood arsenite levels**

420 Building on these findings, we next evaluated whether the engineered *EcN* could protect the
421 host from dietary arsenite exposure in vivo (**Figure 4E**). Mice were orally gavaged with a dose
422 of engineered *EcN*; as controls, two additional groups received either wild-type *EcN* or no
423 bacteria. One hour later, all mice were gavaged with 1 nmol of sodium arsenite, and blood
424 samples were collected at 1, 4, 8, and 24 hours. At every time point, blood arsenite levels in the
425 wild-type *EcN* and no-bacteria groups were comparable, indicating that unmodified *EcN* lacks
426 endogenous pathways capable of reducing arsenite absorption through the gastrointestinal
427 tract.

428 In contrast, mice treated with engineered *EcN* showed a pronounced reduction in arsenite
429 uptake. Four hours after arsenite exposure, blood arsenite levels in the engineered *EcN* group
430 were 4.5 ± 1.6 ppb, significantly lower than those in mice given wild-type *EcN* (37.4 ± 9.1 ppb)
431 or no bacteria (34.5 ± 10.7 ppb). This protective effect persisted at the 8-hour time point, with
432 engineered *EcN*-treated mice maintaining low arsenite levels (4.3 ± 1.0 ppb) compared to wild-
433 type *EcN* (33.5 ± 4.0 ppb) and no-bacteria controls (33.1 ± 3.1 ppb). By 24 hours, arsenite was
434 undetectable in the blood of mice treated with engineered *EcN*, whereas low but measurable
435 levels remained in the wild-type *EcN* (4.2 ± 1.0 ppb) and no-bacteria (4.7 ± 1.0 ppb) groups.

436 Together, these results demonstrate that the engineered *EcN* substantially reduces arsenite
437 absorption from the gastrointestinal tract, supporting the conclusion that sequestration occurred
438 in situ and effectively prevented arsenite from entering the bloodstream.

439

440 **Discussion:**

441 **Important features in our strategy**

442 In this study, we present a microbial sense-and-response strategy that enables selective
443 sequestration of arsenite in the gastrointestinal tract before systemic absorption occurs. By
444 engineering a gut bacterial strain with a synthetic toggle switch controlling expression of a
445 protein-based arsenite chelator, we demonstrate an approach that is both preventative and
446 targeted for managing dietary arsenic exposure. Our results in a mouse model show that a

447 single dose of engineered bacteria before an arsenite exposure can markedly reduce entry of
448 this heavy metal species into the bloodstream, establishing a functional proof of concept for
449 probiotic-based detoxification.
450 A key innovation of our design is the integration of arsenite sensing with dynamically
451 regulated chelator expression. Unlike conventional chelator therapies, which may remove both
452 toxic and essential metal ions, our engineered bacteria activate chelator production only upon
453 detection of arsenite. This conditional expression has several advantages. First, it minimizes off-
454 target depletion of essential micronutrients, a major limitation of prophylactic chelation therapy
455 (*54*). Second, it reduces the baseline metabolic burden on the bacteria, improving their fitness
456 and persistence in the gastrointestinal tract. Third, the use of a toggle switch transforms a
457 transient environmental signal into a sustained protective response, allowing cells to continue
458 detoxifying even after arsenite levels decline—effectively extending the intervention window
459 during the digestive process.
460 The H48A mutant of ArsR, developed here as a DNA-binding-deficient yet high-affinity
461 arsenite chelator, further contributes to the efficiency and safety of this engineered activity. This
462 design prevents unintended transcriptional repression of endogenous genes of the bacteria
463 while retaining strong metal-binding capability. The resulting genetic modularity highlights a
464 broader principle: protein-based chelation can be rationally tuned for performance, opening the
465 door to engineering microbial systems that target other toxic metals or environmental
466 contaminants.
467 Another unique feature of the system is its built-in growth-dependent shutoff mechanism. As
468 the ON-state maintenance depends on cellular CelR levels that are diluted during active cell
469 division, the circuit automatically resets under growth conditions. This behavior prevents long-
470 term, unchecked chelator production in bacteria that may transiently colonize the gut—an
471 important biosafety advantage for living therapeutics intended for repeated administration.
472 Finally, our combined experimental and mathematical modeling framework allowed us to
473 determine bacterial dosing parameters needed for effective in vivo function. This quantitative
474 approach provides a foundation for rational design of microbial detoxifiers and may be
475 applicable to other xenobiotic sequestration problems.
476 With these features, our platform suggests a path toward practical, consumer-friendly
477 strategies for mitigating chronic dietary exposure to toxic metals. As *EcN* is already used as a
478 probiotic supplement in humans (*55*), an engineered version could, in principle, be formulated
479 similarly, as capsules or suspensions taken daily or immediately before meals. Each dose would
480 perform a single-pass detoxification by capturing heavy metals present in the ingested food and

481 directing them toward fecal elimination, thereby reducing the cumulative body burden over time.
482 This approach could be especially valuable in regions where groundwater and food sources are
483 chronically contaminated with arsenite, or in populations for whom dietary control is difficult to
484 maintain. Although translating such a product will require rigorous safety, stability, and regulatory
485 assessments, the combination of selective activation, finite persistence, and defined dosing
486 makes a daily-use formulation both conceptually feasible and potentially transformative as a
487 preventative tool for environmental health.

488 **Limitations and challenges**

489 While our results are encouraging, there are gaps and challenges that require to be
490 overcome for robust applications. In our in vivo experiments, arsenite was administered only
491 one hour after delivery of the engineered bacteria, when the bacterial concentration in the
492 stomach is expected to remain high and the genetic circuit fully active. Under these conditions,
493 we could robustly demonstrate proof-of-concept detoxification. However, further studies are
494 required to evaluate how rapidly the engineered strain is cleared from the stomach, how long
495 the cells remain in a physiologically active state, and how the protective effect decays over time.
496 Future studies will need to quantify the temporal window of efficacy by tracking bacterial
497 persistence, circuit activation dynamics, and sequestration capacity over extended periods
498 following administration. Such data will be essential for informing dosing strategies, predicting
499 real-world performance, and optimizing formulations aimed at routine or pre-meal use.

500 Additionally, regulatory concerns surrounding release, colonization, and clearance of
501 genetically modified organisms must be considered (*56*). Although our growth-dependent shutoff
502 offers an inherent safety mechanism, additional biocontainment systems or exclusively non-
503 colonizing strains may be required for clinical deployment (*57, 58*).

504

505 **Materials and Methods:**

506 **Bacterial strains.** For cloning and construction of genetic circuits, *E. coli XL1-Blue* was
507 used as the plasmid host and cultured in Luria-Bertani (LB) medium. Screening and
508 characterization of arsenite chelator genes were performed in *E. coli BL21-AI*, while
509 characterization of genetic circuits was conducted in *E. coli Nissle* 1917 grown in M9 medium,
510 which consisted of 1× M9 salts, 2 mM $MgSO_4$, 0.1 mM $CaCl_2$, 0.2% (w/v) glucose, and 0.2%
511 (w/v) casamino acids. Unless otherwise specified, all cultures were incubated at 37 °C with
512 shaking at 200 rpm in the presence of kanamycin (50 μg/mL). All chemicals and bacterial culture
513 reagents were purchased from VWR (Radnor, PA) and Thermo Fisher Scientific (Waltham, MA).

514 **Mouse model.** All animal procedures were approved by the University of North Texas
515 Institutional Animal Care and Use Committee (Protocol #24007) and conducted in the Animal
516 Vivarium at the University of North Texas.
517 Experiments were carried out using male C57BL/6 mice aged 7–8 weeks (Charles River,
518 Wilmington, MA). Animals were housed in a specific pathogen–free barrier facility maintained at
519 30–70% humidity and 20–26°C, under a 12:12 h light–dark cycle. Mice were provided feed
520 (Purina Conventional Mouse Diet, JL Rat/Mouse 6F Auto, #5K67) and water ad libitum. Each
521 cage contained four mice, which served as four biological replicates for an experimental
522 condition.
523 **Plasmid construction.** Cloning was performed using standard molecular biology
524 techniques with reagents from New England Biolabs (Ipswich, MA), including Phusion™ High-
525 Fidelity DNA Polymerase, T4 DNA ligase, and the restriction enzymes listed below. The
526 sequence of plasmid selected in each step was deposited in GenBank database.
527 To construct the control circuit in which ArsR regulates mCherry expression (**Figure 2A**), we
528 used plasmid *pTR* from our previous study (*59*) as the backbone. This plasmid contains a
529 kanamycin resistance cassette and a *ColE1* origin of replication. A synthetic DNA fragment
530 containing the *arsR* and mCherry genes, along with their respective promoters and terminators,
531 was inserted into *pTR* via the *PstI* and *MluI* restriction sites using Golden Gate assembly with
532 the endonuclease BsaI-HFv2. These two restriction sites were eliminated at the ligation junction.
533 The sequence of the resulting plasmid has been deposited in GenBank.
534 The arsenite-responsive toggle switch (**Figure 2A** and **Supplementary Figure S1**) was
535 constructed from this control circuit by inserting a fragment containing the *celR* gene driven by
536 the P_{LarsO} promoter and its downstream promoter through the *SalI* and *AflII* sites. Expression of
537 CelR was subsequently optimized by varying its ribosome binding site (RBS) between the *NheI*
538 and *SacI* restriction sites. The optimized toggle-switch circuit sequence is available in GenBank.
539 To enhance output expression, we next incorporated T7 RNA polymerase into the toggle
540 switch (**Figure 2E** and **Supplementary Figure S2**). The T7 RNA polymerase gene fragment
541 replaced mCherry via the *AvrII* and *XhoI* restriction sites. A T7 promoter-mCherry-terminator
542 fragment was then introduced using Golden Gate assembly with endonuclease BsaI-HFv2 to
543 process the insert, which was ligated into the plasmid via *SalI* and *NcoI* (this *NcoI* site was not
544 present in the product upon ligation). This mCherry cassette served as the reporter to
545 characterize T7 polymerase activity. We further optimized T7 RNA polymerase expression by
546 swapping its RBS between the KasI and AvrII sites. The finalized plasmid sequence has been
547 deposited in GenBank.

548 This optimized circuit was subsequently used to drive chelator expression by replacing
549 *mcherry* with the *arsR H48A* gene fragment via *NcoI* and *HindIII*, yielding the final construct
550 shown in **Figure 1** (Accession Number PX644048).
551 To construct the arabinose-inducible system for expressing chelator derivatives (**Figures 3C**
552 and **1D**), the plasmid *pET28b(+)* (*60*) was modified to generate a new vector, designated
553 *pETnoL*. The original *pET28b(+)* plasmid contains a *T7* promoter with a *lac* operator for
554 transcriptional regulation by LacI. To eliminate LacI-mediated repression, the lac operator was
555 removed by replacing the promoter region between the *BglII* and *XbaI* restriction sites, resulting
556 in a *T7* promoter unresponsive to LacI. The *arsR* gene was subsequently cloned into *pETnoL*
557 via *NcoI* and *HindIII* restriction sites. The resulting plasmid, *pETnoL-arsR* served as the
558 template for generating ArsR variant constructs through site-directed mutagenesis using the
559 QuikChange™ method.
560 **Screening of Toggle Switch circuit variants.** To identify the toggle switch variant with the
561 desired response behavior (**Supplementary Figure S1**), each *EcN* strain harboring a circuit
562 variant was grown overnight in M9 medium and then diluted 100-fold into 3 mL of fresh medium
563 containing either 0 or 5 μM sodium arsenite. Cultures were incubated for 24 hours, after which
564 samples were collected for flow cytometry analysis to quantify cellular mCherry fluorescence.
565 Cultures exposed to 5 μM arsenite were then centrifuged to collect the cell pellet, washed once,
566 and resuspended in 3 mL of fresh medium without arsenite, followed by an additional 24-hour
567 incubation before a second mCherry measurement was performed.
568 **Characterization of Toggle Switch.** To assess circuit sensitivity to arsenite (**Figure 2B**),
569 overnight cultures of engineered *E. coli* were diluted 100-fold into 3 mL of fresh M9 medium
570 containing a range of sodium arsenite concentrations (0, 0.16, 0.31, 0.63, 1.25, 2.5, or 5 μM).
571 Cultures were incubated under standard growth conditions for 24 hours, after which cellular
572 mCherry fluorescence was quantified by flow cytometry. Data were analyzed using GraphPad
573 Prism v7.05 and fitted to a nonlinear regression dose-response curve described by the
574 equation:

575 $$S = S_0 + \frac{S_{max} - S_0}{1 + 10^{(logEC_{50} - x)H_s}}$$

576

577 where S_0 and S_{max} represent the basal and maximal mCherry fluorescence, respectively; S is
578 the observed fluorescence signal; x is the logarithm of arsenite concentration; and EC_{50} and H_s
579 (Hill slope) are constants derived from the fit.

580 To characterize the kinetics of output expression in response to arsenite (**Figure 2C**), mid-
581 log phase cultures ($OD_{600} \approx 0.6$) were exposed to 5 μM sodium arsenite. Samples were
582 collected at 0, 0.5, 1, 2, 3, and 4 hours post-induction, and cellular mCherry fluorescence was
583 quantified by flow cytometry.
584 The specificity of signal detection was assessed by diluting overnight cultures of *EcN*
585 harboring the toggle switch plasmid 100-fold into fresh M9 medium supplemented with one of 16
586 test chemicals, as shown in **Figure 2D**. Cultures were incubated under standard growth
587 conditions for 24 hours before flow cytometric analysis to determine cellular mCherry
588 fluorescence.
589 To evaluate the stability of output expression under biostatic conditions (**Figure 2E**),
590 overnight cultures of cells carrying the toggle switch circuit were first diluted 100-fold and then
591 induced with 5 μM sodium arsenite. After overnight incubation (3 mL cultures), cellular mCherry
592 levels were measured with flow cytometry; each culture was centrifuged to collect a cell pellet,
593 which was washed once, and resuspended in an equal volume of fresh M9 medium to continue
594 the incubation. This flow cytometric analysis and medium exchange were repeated every 24
595 hours for 3 days (72 hours total).
596 For experiments assessing the effect of cell growth on output expression
597 (**Supplementary Figure S2**), induced overnight cultures were also washed and resuspended in
598 fresh M9 medium as described above (**Figure 2E**); additionally, cultures were diluted 2-, 3-, or
599 6-fold after each resuspension by mixing 1.5, 1, or 0.5 mL of the culture, respectively, with fresh
600 medium to a final volume of 3 mL. Samples were collected before each medium exchange (0,
601 24, 48, and 72 hours after arsenite removal) for flow cytometric analysis.
602 To characterize toggle switch performance when coupled to the T7 expression system
603 (**Supplementary Figure S3** and **Figure 2F**), mid-log phase cultures were exposed to 0 or 5 μM
604 sodium arsenite, and cell samples were collected after 1 and 24 hours of induction for
605 fluorescence measurement by flow cytometry.
606 **Cellular fluorescence measurement by flow cytometry.** To prepare samples for flow
607 cytometry, 1 to 2 μL of cell culture was diluted in 150 μL of phosphate-buffered saline (PBS).
608 The samples were analyzed using an ACEA NovoCyte 3000VYB flow cytometer (ACEA
609 Biosciences, Inc.). For each experiment, at least 10,000 events were collected and gated based
610 on forward and side scatter to exclude cell debris and aggregates. The geometric mean of
611 fluorescence intensity for each sample was calculated using NovoExpress software (version
612 1.4.1; ACEA Biosciences, Inc.).

613 **Analysis of ArsR/SmtB family regulators.** The NolR-DNA structure in **Figure 3A** was
614 studied with the software PyMol v2.5. Sequence alignment (**Supplementary Figure S4**) was
615 performed with an online tool, Clustal Omega (https://www.ebi.ac.uk/jdispatcher/msa/clustalo).
616 **Engineering of arsenite chelator.** To evaluate the cytotoxicity of ArsR derivatives (**Figure**
617 **3B**), each *pETnoL* plasmid harboring an *arsR* mutant gene was transformed into *E. coli BL21-*
618 *AI*, which carries an arabinose-inducible T7 RNA polymerase gene in its genome. Thus,
619 arabinose addition induces ArsR expression in these cells. Cells containing a *pETnoL* plasmid
620 without arsR gene were used as the control. Overnight cultures in LB medium were diluted
621 1:100 into 3 mL of fresh medium and grown to an OD_{600} of 0.5. A 10 μL aliquot from each culture
622 was collected for colony-forming unit (CFU) analysis prior to induction, after which arabinose
623 was added to a final concentration of 0.2% (w/v) to induce expression. Following 3 hours of
624 induction, another 10 μL sample was taken for CFU determination. For CFU analysis, each
625 sample was serially diluted 10-fold in phosphate-buffered saline (PBS), and 10 μL of each
626 dilution was spotted onto LB agar plates containing kanamycin. Plates were incubated at 37 °C
627 to allow colony formation.
628 To assess arsenite sequestration (**Figure 3C**), each strain was cultured in 5 mL of LB
629 medium until reaching an OD_{600} of 0.5. Each culture was then divided into two 2-mL aliquots;
630 one supplemented with 0.2% (w/v) arabinose (induced) and the other without arabinose
631 (uninduced). After 3 hours of incubation, cells were harvested by centrifugation, washed, and
632 resuspended in PBS containing 20 μM sodium arsenite. Following a 1-hour incubation,
633 supernatants were collected for arsenite quantification by atomic absorption spectroscopy
634 (AAS).
635 **Arsenite quantification by atomic absorption spectroscopy.** Arsenite concentrations
636 were quantified using a Thermo Fisher Scientific iCE™ 3500 Atomic Absorption Spectrometer
637 equipped with a GFS35Z graphite furnace/autosampler. Data acquisition, standard curve fitting,
638 and quantification analysis were performed using SOLAAR v3.0 software. Samples (**Figure 1D**)
639 were diluted 8-fold with fresh PBS, and 1 mL of the diluted sample was mixed with 10 μL of
640 TraceMetal™ grade nitric acid (Thermo Fisher Scientific; Cat. No. A509P500). For calibration,
641 two stock solutions (0 and 5 μM sodium arsenite) were prepared in 1:100 nitric acid/PBS (v/v)
642 and used by the instrument to generate standard concentrations of 0, 0.075, 0.15, 0.325, 0.625,
643 1.25, 2.5, and 5 μM arsenite; results from these standards were used to plot a quadratic
644 standard curve for determine arsenite concentrations in biological samples. During data
645 acquisition, the instrument automatically mixed 20 μL of each sample with 5 μL of the matrix
646 modifier Specpure™ nickel nitrate (Thermo Fisher Scientific; Cat. No. AA39043AE) and

647 processed them according to the graphite furnace parameters listed in **Table 1**. Absorbance
648 was measured for 3 seconds in the Atomization phase at 193.7 nm with a band-pass of 0.5 nm,
649 lamp current set to 90%, and Zeeman background correction applied.
650

Table 1. Graphite furnace parameters for arsenite quantification.

Phase	Temperature (ºC)	Hold time (sec)	Ramp (ºC/sec)	Gas type	Gas flow (L/min)
Drying	100	30	10	Argon	0.2
Ashing	1300	20	150	Argon	0.2
Atomization	2600	3	Max. rate	N/A	Off
Tube clean	2700	3	Max. rate	Argon	0.2

651
652 **Characterization of cell growth.** To evaluate how the arsenite-sequestration circuit affects
653 cellular fitness, we compared the growth of engineered *EcN* containing the toggle switch-
654 arsenite chelator circuit to that of a wild-type *EcN* strain without the plasmid (**Figure 4A**); the
655 wild-type strain did not have the kanamycin-resistance marker and it was grown in M9 media
656 without the antibiotic. Overnight cultures were diluted 1:100 into 5 mL of fresh M9 medium and
657 allowed to grow for 1 hour under standard conditions. Sodium arsenite was then added to a final
658 concentration of either 0 or 5 μM, marking the 0-hour time point. At 0, 0.5, 1, 1.5, 2, 2.5, 3, 3.5,
659 4, 4.5, 5, and 5.5 hours post-addition, 200 μL of culture was transferred into a 96-well plate, and
660 absorbance at 600 nm was measured using a Synergy H1 microplate reader (Agilent
661 Technologies). Growth rates were calculated using the following equation:

662 $$Growth\ rate = \frac{\log(\mathrm{OD600_f}) - \log(\mathrm{OD600_i})}{\mathrm{Time_f} - \mathrm{Time_i}}$$

663
664 where $OD600_f$ and $Time_f$ correspond to measurements at the 4-hour time point, and $OD600_i$ and
665 $Time_i$ correspond to the 0.5-hour time point. These time points were selected because the
666 cultures exhibited clear exponential growth during this interval. To assess viable cell density,
667 samples were also collected at 0.5, 3, and 5.5 hours for CFU analysis (**Supplementary Figure**
668 **S5**).
669 **In vitro characterization of arsenite sequestration.** To quantify the rate of arsenite
670 sequestration (**Figure 4B**), engineered *EcN* cultures were grown in 5 mL of M9 medium to an
671 OD600 of approximately 0.7. Sodium arsenite was then added to a final concentration of 5 μM.
672 At 0, 0.5, 1, 2, 3, and 4 hours post-addition, 300 μL of each culture was collected, centrifuged,

673 and the supernatant was analyzed by inductively coupled plasma mass spectrometry (ICP-MS)
674 to determine arsenite concentrations. CFU measurements were performed at 0, 1, 2, 3, and 4
675 hours to estimate viable cell density (**Supplementary Figure S6**).
676 To determine the arsenite sequestration capacity (**Figure 4C**), cultures at OD600 ≈ 0.7 were
677 exposed to 20 μM sodium arsenite, and samples were collected at 0 and 3 hours for ICP-MS
678 analysis. CFU counts were obtained at both time points (**Supplementary Figure S6**).
679 **Mass transfer simulations.** We developed a mathematical model to simulate the transfer of
680 arsenite from the stomach lumen into engineered bacteria and gastrointestinal epithelial cells
681 (**Figure 4D**). To simplify the system, we assumed that: (i) neither arsenite nor bacterial cells exit
682 the stomach compartment; (ii) arsenite internalized by cells does not return to the lumen; and
683 (iii) the total amounts of arsenite, engineered bacteria, and epithelial cells remain constant over
684 time. Under these assumptions, we described the time-dependent distribution of arsenite across
685 the three compartments using the following equations:
686 Equation 1; change of arsenite concentration in the gut lumen:

687 $$\frac{dC_g(t)}{dt} = (-Vn_b \underbrace{k_b C_g(t)}_{\substack{Uptake\ by \\ Bacteria}} - AN_e \underbrace{k_e C_g(t)}_{\substack{Uptake\ by \\ epithelial\ cells}})$$

688

689 Equation 2; contribution of bacterial cells to the change of arsenite concentration in the gut lumen:

690 $$\frac{dC_b(t)}{dt} = Vn_b \underbrace{k_b C_g(t)}_{\substack{Uptake\ by \\ one\ bacteria}}$$

691

692 Equation 3, contribution of epithelial cells to the change of arsenite concentration in the gut lumen:

693 $$\frac{dC_e(t)}{dt} = AN_e \underbrace{k_e C_g(t)}_{\substack{Uptake\ by \\ one\ epithelial\ cell}}$$

694

695 Where $C_g(t)$ is the concentration of arsenite (μM) in the stomach lumen, and $C_b(t)$ and $C_e(t)$ are
696 the contributions of bacterial cells and epithelial cells, respectively, to the decrease in arsenite in
697 the stomach lumen; k_b and k_e are bacteria and epithelial cell uptake rate coefficient; V is
698 stomach volume, n_b is bacterial cell density; A is the gut interior wall area; and N_e is the number
699 of epithelial cells per unit area of gut wall.

By solving these equations, we derive explicit expressions (Equations 4 to 6) that predict the temporal concentration of arsenite in lumen, bacteria, and epithelial cells as a function of bacterial cell number.

Equation 4:

$$C_g(t) = C_0 e^{-(Vn_b k_b + AN_e k_e)t}$$

Equation 5:

$$C_b(t) = \frac{Vn_b k_b C_0}{Vn_b k_b + AN_e k_e}(1 - e^{-(Vn_b k_b + AN_e k_e)t})$$

Equation 6:

$$C_e(t) = \frac{AN_e k_e C_0}{Vn_b k_b + AN_e k_e}(1 - e^{-(Vn_b k_b + AN_e k_e)t})$$

In these equations, the bacterial cell density, n_b (cells mL^{-1}), and time, t (hour), are variables. The values of all epithelial cells-related parameters were obtained from the literature: gut surface area, A, is 1.4×10^6 mm^2 (*61*). Lumen volume, V, is 0.4 mL (*52*). Arsenite uptake rate coefficient of epithelial cells is reported as 0.11 h^{-1} (*50*); in this study, it was normalized on a per-cell, per-hour basis to yield $k_e = 0.11 \times 10^{-10}$ h^{-1} $cell^{-1}$. The epithelial cell density on the gut wall, N_e, was estimated to be 1.9×10^4 cells mm^{-2} based on published data (*53*).

The arsenite uptake rate coefficient, k_b, was estimated from our experimental data in **Figure 4B** with the following equation:

$$k_b = -\frac{ln\frac{C(t_f)}{C(t_i)}}{t_f - t_i}$$

Where *C(t)* is the concentration of arsenite in the supernatant at time t. We used data from timepoints 1-hour and 2-hour to calculate k_b, which resulted as 6.3×10^{-10} $cell^{-1}$ h^{-1}.

These parameters were then used to compute values of $C_g(t)$, $C_b(t)$, and $C_e(t)$ by using MATLAB R2023b. Results with bacterial cells number, Vn_b = 1, 5, and 10×10^9 cells were plotted (**Figure 4D**).

Animal studies. All mice were quarantined in the animal facility for at least one week prior to experimentation. To characterize dose-dependent arsenite absorption (**Supplementary**

728 **Figure S7**), each mouse received 100 μL of sodium arsenite solution (10 or 40 μM) by oral
729 gavage, corresponding to a total dose of 1 or 4 nmol of arsenite. Blood samples (100 μL) were
730 collected from the tail vein using a 25-gauge needle at 1, 4, 8, and 24 hours after gavage. To
731 prevent clotting, each sample was immediately mixed with 10 μL of 2% (w/v) EDTA. Samples
732 were then centrifuged to isolate plasma for ICP-MS analysis.

733 To assess the effect of engineered *EcN* on arsenite absorption (**Figure 4E**), *EcN* cultures
734 were grown in M9 medium to an OD600 of ~0.7, corresponding to an estimated density of ~5
735 $\times 10^9$ cells/mL. For each mouse, 1 mL of culture was centrifuged, and the resulting pellet was
736 resuspended in 100 μL of PBS for oral gavage. One hour later, mice received arsenite, and
737 blood collection proceeded, following the same protocol used in the dose-dependent absorption
738 study (**Supplementary Figure S7**).

739 Statistical analysis of animal studies was performed with the software, GraphPad Prism
740 v7.0.5. A two-way ANOVA was conducted with treatment and time as independent variables and
741 blood metal levels as the dependent variable, testing for the two main effects (treatment and
742 time) and their interactions to determine whether the temporal trajectory of blood metal levels
743 differed across groups. Significant effects were followed by post hoc pairwise comparisons with
744 correction for multiple testing (e.g., Tukey's HSD) to identify specific time points and treatment
745 groups that differ.

746 **Inductively Coupled Plasma Mass Spectrometry.** ICP-MS analysis was performed with
747 an Agilent LC-linked ICP-MS 7850 with dual autosamplers (Agilent Technologies). It was
748 operated under the following optimized conditions: radio frequency (RF) power of 1550 W,
749 plasma gas flow of 15 mL/min, auxiliary gas flow of 0.9 mL/min, and nebulizer gas flow rate of
750 1.08 L/min. These parameters ensured stable plasma conditions, efficient ionization of analytes,
751 and high analytical sensitivity. For sample preparation, 50 μL of each blood plasma sample was
752 mixed with 5 mL of a diluent containing 0.5% HNO_3 and 2% ethanol (v/v). The diluted mixture
753 was vortexed thoroughly to ensure complete homogenization and then analyzed on the same
754 day to minimize degradation. Matrix-matched calibration solutions were prepared from the multi-
755 element stock standard (Inorganic Ventures, Christiansburg, VA) in 0.5% HNO_3 and 2% ethanol
756 (v/v), using pooled blood plasma from exposed mice to account for matrix effects of blood
757 analysis with calibration levels set at 0.01, 0.1, 0.5, 1, 2.5, 5 and 15 μg/L. An internal standard
758 solution containing 1 μg/mL yttrium (Y), was continuously introduced into the system throughout
759 the analysis. The regression coefficient of the calibration curve above 0.995, was accepted for
760 quantification. The detection limit for arsenic was 0.018 μg/L (2.34×10^{-4} μM).

Graphical illustrations. We used two images from NIH BioArt Source to create figures, including [NIAID Visual & Medical Arts. (10/7/2024). Bacillus Bacteria. NIAID NIH BIOART Source. bioart.niaid.nih.gov/bioart/43]; and [NIAID Visual & Medical Arts. (10/7/2024). Basal Cell Brush. NIAID NIH BIOART Source. bioart.niaid.nih.gov/bioart/45].

References

1. Y. S. Hong, K. H. Song, J. Y. Chung, Health effects of chronic arsenic exposure. *J Prev Med Public Health* **47**, 245-252 (2014).
2. M. F. Naujokas *et al.*, The broad scope of health effects from chronic arsenic exposure: update on a worldwide public health problem. *Environ Health Perspect* **121**, 295-302 (2013).
3. UNICEF, Arsenic primer: guidance on the investigation & mitigation of arsenic contamination. *New York*, (2018).
4. J. D. Ayotte, L. Medalie, S. L. Qi, L. C. Backer, B. T. Nolan, Estimating the high-arsenic domestic-well population in the conterminous United States. *Environmental science & technology* **51**, 12443-12454 (2017).
5. B. Arslan, M. B. A. Djamgoz, E. Akun, ARSENIC: A Review on Exposure Pathways, Accumulation, Mobility and Transmission into the Human Food Chain. *Rev Environ Contam Toxicol* **243**, 27-51 (2017).
6. D. Wang *et al.*, Impact of climate change on arsenic concentrations in paddy rice and the associated dietary health risks in Asia: an experimental and modelling study. *Lancet Planet Health* **9**, e397-e409 (2025).
7. F. I. Hassan, K. Niaz, F. Khan, F. Maqbool, M. Abdollahi, The relation between rice consumption, arsenic contamination, and prevalence of diabetes in South Asia. *EXCLI J* **16**, 1132-1143 (2017).
8. T. Macek, M. Mackova, J. Kas, Exploitation of plants for the removal of organics in environmental remediation. *Biotechnol Adv* **18**, 23-34 (2000).
9. S. Pattnaik, M. V. Reddy, Assessment of municipal solid waste management in Puducherry (Pondicherry), India. *Resources, Conservation and Recycling* **54**, 512-520 (2010).
10. V. Misra, S. D. Pandey, Hazardous waste, impact on health and environment for development of better waste management strategies in future in India. *Environ Int* **31**, 417-431 (2005).
11. E. Erdemir *et al.*, Rapid, ultrasensitive, highly selective detection of toxic Hg(II) ions in seabass, swordfish and water samples. *Food Chem* **371**, 131309 (2022).
12. W. Guo, S. Hu, Y. Xiao, H. Zhang, X. Xie, Direct determination of trace cadmium in environmental samples by dynamic reaction cell inductively coupled plasma mass spectrometry. *Chemosphere* **81**, 1463-1468 (2010).
13. D. N. Karaman, H. Serbest, Y. Kilinç, R. Demirel, S. Bakırdere, Trace cadmium determination in lake water matrix by flame atomic absorption spectrometry after manganese ferrite magnetic nanoparticles-based dispersive solid phase extraction. *CLEAN–Soil, Air, Water*, 2200186 (2023).
14. M. Soylak, M. Alasaad, Ö. Özalp, Fabrication and characterization of MgCo2O4 for solid phase extraction of Pb (II) from environmental samples and its detection with high-resolution continuum source flame atomic absorption spectrometry (HR-CS-FAAS). *Microchemical Journal* **178**, 107329 (2022).

15. A. Rihana-Abdallah, Z. Li, K. C. Lanigan, Using Cloud Point Extraction for Preconcentration and Determination of Iron, Lead, and Cadmium in Drinking Water by Flame Atomic Absorption Spectrometry. *Analytical Letters* **55**, 1296-1305 (2022).
16. C. Ornillo, N. Harbord, Fundaments of Toxicology-Approach to the Poisoned Patient. *Adv Chronic Kidney Dis* **27**, 5-10 (2020).
17. S. Singh, A. Mulchandani, W. Chen, Highly selective and rapid arsenic removal by metabolically engineered Escherichia coli cells expressing Fucus vesiculosus metallothionein. *Appl Environ Microbiol* **74**, 2924-2927 (2008).
18. V. Jafarian, F. Ghaffari, A unique metallothionein-engineered in Escherichia coli for biosorption of lead, zinc, and cadmium; absorption or adsorption? *Microbiology+* **86**, 73-81 (2017).
19. S. Chen, D. B. Wilson, Genetic engineering of bacteria and their potential for Hg2+ bioremediation. *Biodegradation* **8**, 97-103 (1997).
20. W. Bae, R. K. Mehra, A. Mulchandani, W. Chen, Genetic engineering of Escherichia coli for enhanced uptake and bioaccumulation of mercury. *Appl Environ Microbiol* **67**, 5335-5338 (2001).
21. T. Yang, J. W. Liu, C. B. Gu, M. L. Chen, J. H. Wang, Expression of Arsenic Regulatory Protein in Escherichia coli for Selective Accumulation of Methylated Arsenic Species. *Acs Appl Mater Inter* **5**, 2767-2772 (2013).
22. K. T. Kitchin, K. Wallace, Arsenite binding to synthetic peptides based on the Zn finger region and the estrogen binding region of the human estrogen receptor-alpha. *Toxicol Appl Pharmacol* **206**, 66-72 (2005).
23. P. Kolkowska *et al.*, Specificity of the Zn(2+), Cd(2+) and Ni(2+) ion binding sites in the loop domain of the HypA protein. *Dalton Trans* **44**, 9887-9900 (2015).
24. K. Krzywoszynska *et al.*, Polythiol binding to biologically relevant metal ions. *Dalton Trans* **40**, 10434-10439 (2011).
25. K. De Mora *et al.*, A pH-based biosensor for detection of arsenic in drinking water. *Analytical and Bioanalytical chemistry* **400**, 1031-1039 (2011).
26. J. Aleksic *et al.*, Development of a novel biosensor for the detection of arsenic in drinking water. *IET Synthetic biology* **1**, 87-90 (2007).
27. H.-C. Tao, Z.-W. Peng, P.-S. Li, T.-A. Yu, J. Su, Optimizing cadmium and mercury specificity of CadR-based E. coli biosensors by redesign of CadR. *Biotechnology letters* **35**, 1253-1258 (2013).
28. R. Branco, A. Cristovao, P. V. Morais, Highly sensitive, highly specific whole-cell bioreporters for the detection of chromate in environmental samples. *PLoS One* **8**, e54005 (2013).
29. Y. Cai *et al.*, Evolved Biosensor with High Sensitivity and Specificity for Measuring Cadmium in Actual Environmental Samples. *Environ Sci Technol* **56**, 10062-10071 (2022).
30. L. Li *et al.*, Evolved bacterial biosensor for arsenite detection in environmental water. *Environ Sci Technol* **49**, 6149-6155 (2015).
31. X. Wan *et al.*, Cascaded amplifying circuits enable ultrasensitive cellular sensors for toxic metals. *Nat Chem Biol* **15**, 540-548 (2019).
32. A. Cubillos-Ruiz *et al.*, Engineering living therapeutics with synthetic biology. *Nat Rev Drug Discov* **20**, 941-960 (2021).
33. V. M. Isabella *et al.*, Development of a synthetic live bacterial therapeutic for the human metabolic disease phenylketonuria. *Nat Biotechnol* **36**, 857-864 (2018).
34. P. Wei *et al.*, Oral Bifidobacterium longum expressing alpha-melanocyte-stimulating hormone to fight experimental colitis. *Drug Deliv* **23**, 2058-2064 (2016).

35. S. W. Yoon *et al.*, Lactobacillus casei secreting alpha-MSH induces the therapeutic effect on DSS-induced acute colitis in Balb/c Mice. *J Microbiol Biotechnol* **18**, 1975-1983 (2008).
36. S. Liu, Y. Li, B. Deng, Z. Xu, Recombinant Lactococcus lactis expressing porcine insulin-like growth factor I ameliorates DSS-induced colitis in mice. *BMC Biotechnol* **16**, 25 (2016).
37. S. Shigemori *et al.*, Oral delivery of Lactococcus lactis that secretes bioactive heme oxygenase-1 alleviates development of acute colitis in mice. *Microb Cell Fact* **14**, 189 (2015).
38. J. N. V. Martinson, S. T. Walk, Escherichia coli Residency in the Gut of Healthy Human Adults. *EcoSal Plus* **9**, (2020).
39. R. Rosenstein, A. Peschel, B. Wieland, F. Gotz, Expression and regulation of the antimonite, arsenite, and arsenate resistance operon of Staphylococcus xylosus plasmid pSX267. *J Bacteriol* **174**, 3676-3683 (1992).
40. R. P. Dimas, X. L. Jiang, J. Alberto de la Paz, F. Morcos, C. T. Y. Chan, Engineering repressors with coevolutionary cues facilitates toggle switches with a master reset. *Nucleic Acids Res* **47**, 5449-5463 (2019).
41. X. Cheng, T. A. Patterson, Construction and use of lambda PL promoter vectors for direct cloning and high level expression of PCR amplified DNA coding sequences. *Nucleic Acids Res* **20**, 4591-4598 (1992).
42. L. K. Certain, J. C. Way, M. J. Pezone, J. J. Collins, Using Engineered Bacteria to Characterize Infection Dynamics and Antibiotic Effects In Vivo. *Cell Host Microbe* **22**, 263-268 e264 (2017).
43. H. M. Salis, The ribosome binding site calculator. *Methods Enzymol* **498**, 19-42 (2011).
44. S. Ramanathan, W. Shi, B. P. Rosen, S. Daunert, Sensing antimonite and arsenite at the subattomole level with genetically engineered bioluminescent bacteria. *Anal Chem* **69**, 3380-3384 (1997).
45. J. Kostal, R. Yang, C. H. Wu, A. Mulchandani, W. Chen, Enhanced arsenic accumulation in engineered bacterial cells expressing ArsR. *Appl Environ Microbiol* **70**, 4582-4587 (2004).
46. S. G. Lee, H. B. Krishnan, J. M. Jez, Structural basis for regulation of rhizobial nodulation and symbiosis gene expression by the regulatory protein NolR. *Proc Natl Acad Sci U S A* **111**, 6509-6514 (2014).
47. C. Eicken *et al.*, A metal-ligand-mediated intersubunit allosteric switch in related SmtB/ArsR zinc sensor proteins. *Journal of molecular biology* **333**, 683-695 (2003).
48. L. S. Busenlehner, T. C. Weng, J. E. Penner-Hahn, D. P. Giedroc, Elucidation of primary (alpha(3)N) and vestigial (alpha(5)) heavy metal-binding sites in Staphylococcus aureus pI258 CadC: evolutionary implications for metal ion selectivity of ArsR/SmtB metal sensor proteins. *Journal of molecular biology* **319**, 685-701 (2002).
49. M. L. VanZile, X. Chen, D. P. Giedroc, Structural characterization of distinct alpha3N and alpha5 metal sites in the cyanobacterial zinc sensor SmtB. *Biochemistry* **41**, 9765-9775 (2002).
50. S. D. Lawley *et al.*, Mathematical model insights into arsenic detoxification. *Theor Biol Med Model* **8**, 31 (2011).
51. C. Casteleyn, A. Rekecki, A. Van der Aa, P. Simoens, W. Van den Broeck, Surface area assessment of the murine intestinal tract as a prerequisite for oral dose translation from mouse to man. *Lab Anim-Uk* **44**, 176-183 (2010).
52. E. L. McConnell, A. W. Basit, S. Murdan, Measurements of rat and mouse gastrointestinal pH, fluid and lymphoid tissue, and implications for in-vivo experiments. *J Pharm Pharmacol* **60**, 63-70 (2008).

53. S. M. Karam, C. P. Leblond, Identifying and counting epithelial cell types in the "corpus" of the mouse stomach. *Anat Rec* **232**, 231-246 (1992).
54. J. F. Finklea, Prophylactic Chelation Therapy for Lead-Exposure. *Jama-J Am Med Assoc* **235**, 1553-1553 (1976).
55. Z. Zhao, S. Xu, W. Zhang, D. Wu, G. Yang, Probiotic Escherichia coli NISSLE 1917 for inflammatory bowel disease applications. *Food Funct* **13**, 5914-5924 (2022).
56. J. W. Lee, C. T. Y. Chan, S. Slomovic, J. J. Collins, Next-generation biocontainment systems for engineered organisms. *Nat Chem Biol* **14**, 530-537 (2018).
57. N. Nguyen, M. Wang, L. Li, C. T. Y. Chan, A genetic safeguard for eliminating target genes in synthetic probiotics in a gut environment. *iScience* **28**, 113027 (2025).
58. A. G. Rottinghaus, A. Ferreiro, S. R. S. Fishbein, G. Dantas, T. S. Moon, Genetically stable CRISPR-based kill switches for engineered microbes. *Nat Commun* **13**, 672 (2022).
59. X. L. Jiang, R. P. Dimas, C. T. Y. Chan, F. Morcos, Coevolutionary methods enable robust design of modular repressors by reestablishing intra-protein interactions. *Nat Commun* **12**, 5592 (2021).
60. F. W. Studier, B. A. Moffatt, Use of bacteriophage T7 RNA polymerase to direct selective high-level expression of cloned genes. *Journal of molecular biology* **189**, 113-130 (1986).
61. C. Casteleyn, A. Rekecki, A. Van der Aa, P. Simoens, W. Van den Broeck, Surface area assessment of the murine intestinal tract as a prerequisite for oral dose translation from mouse to man. *Lab Anim* **44**, 176-183 (2010).

Acknowledgements

We thank Dr. Brianne Soulen and the UNT Advanced Environmental Research Institute for guidance in performing atomic absorption spectroscopy analyses. We also acknowledge the use of the online tool ChatGPT 5.1 for assistance with grammar and text refinement.

Funding:

NIH/NIGMS grant R35GM142421 (CTYC)

NIH/NIGMS grant R15GM135813 (CTYC)

NIH/NINDS grant R16NS131108 (LL)

Author contributions:

Conceptualization: CTYC

Methodology: NN, MW, SSM, VK, FE, LJS, LL, and CTYC

Investigation: NN, MW, SSM, VK, and FE

Visualization: FE and CTYC

Supervision: FE, LJS, LL, and CTYC

Writing—original draft: CTYC

Writing—review & editing:

Competing Interests:

N.N. and C.T.Y.C. are inventors on a U.S. provisional patent application under 35 USC 111(b) related to the technology described in this article. C.T.Y.C is a co-founder of ModularBio LLC. Other authors declare no competing interests.

Data and Materials Availability

All data needed to evaluate the conclusions in the paper are present in the paper and/or the Supplementary Materials. Sequences of plasmids developed in this study are deposited in GenBank database:

GenBank will release them to the public database until the accession numbers appear in print.